14th International Symposium on Turbulence and Shear Flow Phenomena (TSFP14)
Heidelberg, Germany, July 28–31, 2026

MEAN MOMENTUM BALANCE AND POWER LOSS IN SMOOTH AND ROUGH-WALL PIPE FLOWS LADEN WITH PARTICLES

Jimmy Philip
Department of Mechanical Engineering
The University of Melbourne, Australia
jimmyp@unimelb.edu.au

Leon Chan
Department of Mechanical Engineering,
The University of Melbourne, Australia

Tony Zahtila
Center for Turbulence Research, Stanford University, USA
Department of Mechanical Engineering, The University of Melbourne, Australia

ABSTRACT

With the aim of understanding rough-wall particle-laden pipe flows, appropriately double-averaged mean momentum and mean rate of energy (power) balance equations are derived and analysed with direct numerical simulation (DNS) data of rough and smooth wall pipes, for both particle-laden (in the two-way coupling regime) and unladen cases at a friction Reynolds number $Re_\tau = 180$. Particles act as a momentum sink away from the wall in both smooth and rough cases. However, they act as a source of momentum only in the near-wall region of smooth pipes, because particles transfer net zero momentum in smooth pipes whereas a non-zero momentum is transferred to the walls in rough pipes. While particles reduce turbulent shear stress and consequently turbulent dissipation, energy is still lost in transporting particles in both smooth and rough pipes, which we quantify. We also observe that substantial power is expended in overcoming roughness drag within the canopy; however, this inner region is relatively unaffected by particles, with their effects mostly confined to the the outer region.

1 Introduction

The mean momentum balance (MMB) equation, i.e, streamwise force balance, has been widely used to understand the role of turbulence in various canonical *unladen smooth-walled* flows (e.g., Wei *et al.*, 2005; Morrill-Winter *et al.*, 2017) including pipes (Chin *et al.*, 2014). MMB provides a rational basis for separating the boundary layer into different regions based on the dominant force balance. More recently in Zahtila *et al.* (2026), MMB-based analysis is employed in *particle-laden smooth* pipes and channel to understand the effect of particle-induced forces on the structure of the momentum balance. No such analysis has been conducted for *rough-walled* particle-laden flows. This is partly because, in rough walls, the resulting equations require 'double-averaging' owing to the fluid volume fraction ϕ_f being a function of the wall-distance.

Despite the physical insights provided by MMB analysis, the effect of turbulence on net drag or power cannot be assessed directly from it. A common method to quantify turbulence contribution to the drag is via the 'FIK decomposition', which involves triple-integrating the MMB leading to a decomposition of the drag into contributions from the mean flow and turbulence, and this has been applied to particle-laden channels (Picano *et al.*, 2015; Gualtieri *et al.*, 2023) and pipe flows (Cui *et al.*, 2025, 2026). However, the physical meaning of FIK's split of drag among mean flow, turbulence, and particle-force is a little ambiguous. This is because the net streamwise force exerted by the turbulence (via the Reynolds shear stress) is zero, and, similarly, elastically colliding particles in a steady state cannot exert any net force on the *smooth* pipe or channel walls. Consequently, one might say that the net effect of momentum transfer by turbulence as well as elastic particles on smooth walls should be zero despite the FIK decomposition showing a non-zero contribution. These limitations led Zahtila *et al.* (2026) to focus on the mean energy equation that allows the net power consumed (i.e., the rate at which the input energy is lost) in driving the particle-laden flow to be decomposed into contributions from the mean and turbulent dissipation and the work done in transporting the particles. Rough-walled flows have not yet been considered within this framework.

As such, we have two main objectives. First, we present a force balance analysis of rough-walled, particle-laden pipe flows as a function of wall-distance by developing an appropriate double-averaged MMB equation, and compare it with the smooth-walled case. Second, we develop a double-averaged mean energy equation for rough-wall particle-laden flows, presenting the wall-normal distribution of power loss from different components and comparing them with their unladen and smooth-walled counterparts. The particle-laden flow data is obtained through the DNS of smooth and rough-walled flows with heavy point particles in the two-way coupling regime.

2 DNS Methodology and problem parameters

The governing equations for the particle-laden flow system consists of the fluid part represented (and solved) in the Eulerian framework:

$$\rho\frac{\partial u_i}{\partial t} + \rho u\cdot\nabla u_i = -\frac{\mathrm{d}P}{\mathrm{d}x}\delta_{i1} - \frac{\partial p}{\partial x_i} + \mu\nabla^2 u_i - F_{pi} \quad (1a)$$

$$\nabla\cdot u = 0, \quad (1b)$$

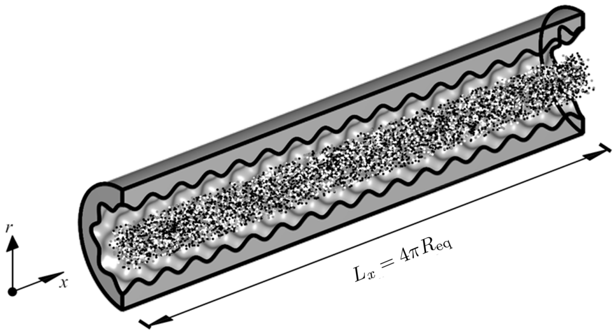

Figure 1. A schematic of the rough-walled pipe used for the particle-laden DNS.

where u_i and p are the fluid velocity and fluctuating pressure, respectively, $\mathrm{d}P/\mathrm{d}x$ is the constant streamwise pressure gradient driving the flow, ρ and μ are the fluid density and dynamic viscosity, and F_{pi} is the particle force (per unit volume) acting on the fluid. The 'point' particles are tracked by their Lagrangian equation,

$$\frac{dx_{pi}}{dt} = u_{pi}, \text{ and, } m_p \frac{du_{pi}}{dt} = F_{di} + F_{li}, \tag{2}$$

where, x_p, u_{pi} and m_p are the particle position, velocity and mass, and the 'computational cell volume averages' of the drag and lift forces $F_{di} + F_{li}$ is equal to F_{pi}. These equations are solved via the open source codes Nek5000 for smooth and in OpenFOAM for the rough-wall cases.

In rough-wall cases, an 'egg-carton' type surface roughness (e.g., see figure 1 and Chan *et al.* (2021)) is considered that has roughness semi-amplitude of 20 viscous units and wavelength of 142 viscous units. For the particle-laden rough-wall case we only include the dominant force owing to drag F_{di}. Spherical particles with diameter d_p and density ρ_p are governed by three non-dimensional numbers: (i) density ratio ρ_p/ρ (=10 000 for our cases), (ii) Stokes number $St^+ = \tau_p/\tau_f$ (where the particle and fluid timescales are $\tau_p = d_p^2 \rho_p/(18\mu)$ and $\tau_f = \nu/u_\tau^2$ with fluid kinematic viscosity ν and friction velocity u_τ based on $\mathrm{d}P/\mathrm{d}x$), and (iii) the particle volume fraction ϕ_{pv}.

All cases are maintained at $Re_\tau = u_\tau R/\nu =: R^+ = 180$, where R is the pipe radius in the smooth wall (superscript + denoting viscous normalisation), and is replaced by an equivalent radius R_{eq} such that the average cross-sectional area of the rough-wall pipe is πR_{eq}^2. DNS of unladen turbulent smooth and rough wall cases were carried out in addition to the particle-laden cases with $St^+ = 500$ and $\phi_{pv} = 2.5 \times 10^{-5}$, whereas for the rough wall case $St^+ = 500$ and $\phi_{pv} = 2 \times 10^{-5}$. The ϕ_{pv} , although slightly different, are close enough to provide relevant insights into the differences between the smooth and rough cases.

3 Mean momentum (or force) balance

We follow the double-averaging technique (e.g., Nikora *et al.*, 2007; Unigarro Villota *et al.*, 2023) but modifying such that the volume average is within a thin ring in the azimuthal–axial direction $V_0 = \phi_f V_f$, where V_f the fluid volume. Applying averaging to (1) in the $x-$ direction results in the MMB equation for a rough particle-laden pipe flow (in the viscous normalisation),

$$\begin{aligned} 0 = \phi_f \frac{2}{R_{\mathrm{eq}}^+} &+ \underbrace{\frac{1}{r^+}\frac{\mathrm{d}}{\mathrm{d}r^+}\left(r^+ \phi_f \langle \overline{\tau_{xr}} \rangle^+\right)}_{\mathrm{TI}} \\ &+ \underbrace{\frac{1}{r^+}\frac{\mathrm{d}}{\mathrm{d}r^+}\left(r^+ \phi_f \frac{\mathrm{d}\phi_f \langle \overline{u_x} \rangle^+}{\mathrm{d}r^+}\right)}_{\mathrm{VF}} \\ &- \phi_f \langle \overline{D_x} \rangle^+ - \phi_f \langle \overline{F_{px}} \rangle^+, \end{aligned} \tag{3}$$

where,

$$\langle \overline{\tau_{xr}} \rangle^+ = -\langle \overline{u_x}'' \overline{u_r}'' \rangle^+ - \langle \overline{u_x' u_r'} \rangle^+ \tag{4a}$$

$$\langle \overline{D_x} \rangle \equiv \frac{1}{V_f} \iint_A \left(-\overline{p}\, n_x + \mu \nabla \overline{u_x} \cdot n\right) \mathrm{d}A, \tag{4b}$$

averaged over the roughness area A touching the fluid in V_f with the normal n pointing from solid to the fluid, $\langle \overline{D_x} \rangle^+ = \frac{\langle \overline{D_x} \rangle}{\rho u_\tau^3/\nu}$ and $\langle \overline{F_{px}} \rangle^+ = \frac{\langle \overline{F_{px}} \rangle}{\rho u_\tau^3/\nu}$. Here an overline is time averaging and primes represent deviations from it, i.e., $u_i(x,r,\theta,t) = \overline{u_i}(x,r,\theta) + u_i'(x,r,\theta,t)$, and angled-brackets are 'intrinsic' averaging within the ring (of volume $V_0 = 2\pi L_x r \Delta r$ with Δr the ring thickness), i.e., $\overline{u_i}(x,r,\theta) = \langle \overline{u_i} \rangle(r) + \overline{u_i}''(x,r,\theta)$. For the smooth-wall cases, in (3), $\phi_f = 1$, $\langle \overline{D_x} \rangle = 0$, R_{eq}^+ is replaced with R^+ and there is only a time-averaging, i.e., $u_i(x,r,\theta,t) = \overline{u_i}(r) + u_i'(x,r,\theta,t)$. For the unladen smooth-wall case $\overline{F_{px}} = 0$ and $\langle \overline{F_{px}} \rangle = 0$ for the unladen rough-wall case. In (3) the TI and VF denote respectively, the turbulent inertia and the mean inertia terms.

Figures 2(a) and (b) respectively show the terms in (3) for smooth and rough wall pipes. Here the unladen and particle-laden cases are respectively presented in solid and dashed lines (accompanied by sparse solid and empty symbols).

In a smooth-walled pipe (c.f., figure 2a), for the unladen case (i.e., D_x and F_{px} are zero), the dominant balance of forces is between the turbulent inertia (TI) and the viscous force (VF) in the near-wall region, where as the TI balances the driving pressure gradient in the outer region, and in-between there is a region where the three terms are in balance. With the addition of particles (which introduces $\overline{F_{px}}$), the outer balance does not seem to be affected by the addition the particles, likely because of the relatively low particle volume fraction; however, $-\overline{F_{px}}$ is slightly negative (i.e., particles are extracting momentum from the fluid) which causes a slight reduction in the TI term. In the near-wall region we observe a more substantial effect of particles, where $-\overline{F_{px}} > 0$, i.e., particles provide momentum to the fluid, which causes a noticeable reduction in TI, whereas VF remains largely unaffected. This is consistent with many studies that report a mean particle velocity that is larger than the mean fluid velocity in the near-wall region and the opposite in the outer-region. Importantly, $\int_0^R \overline{F_{px}}\, r\, \mathrm{d}r = 0$ in the smooth-wall case, that is also confirmed by our DNS, because wall collisions are elastic and no momentum is transferred to the pipe. This means that particles act as a sink of momentum in the outer region, but as a source of momentum as they travel closer to the wall within the slower-moving fluid carrying with themselves the momentum gained in the outer-region. Interestingly, both particles and turbulence behave in a similar manner in the MMB; as a source and sink of momentum in the inner and outer region respectively. Since VF is hardly affected, particles seem to replace turbulence, as far as momentum transport in concerned.

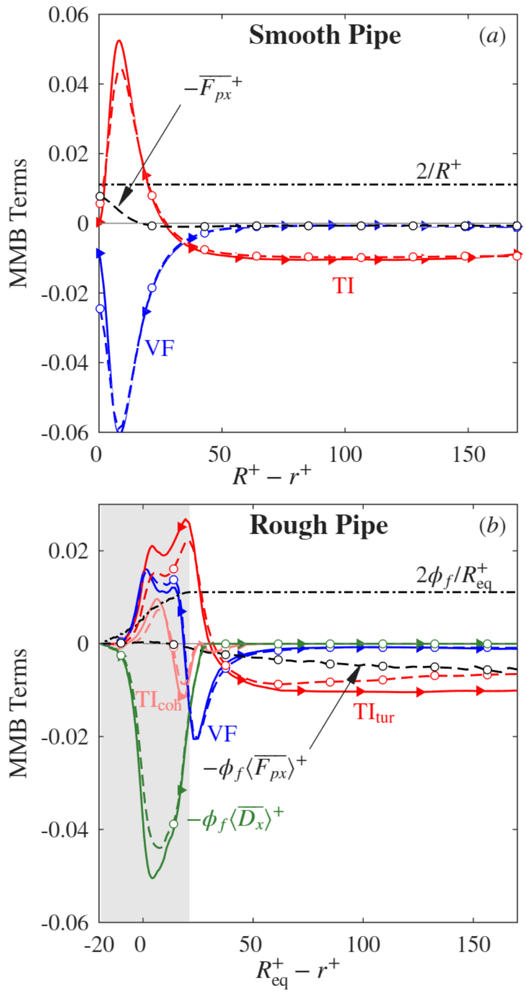

Figure 2. Distribution of the different terms in the MMB balance equation (3) for (a) smooth, and (b) rough pipes. Solid lines are unladen, whereas dashed lines correspond to particle-laden cases. The shaded region in (b) corresponds to the roughness canopy.

The rough-wall case MMB is presented in figure 2(b), and we first consider the unladen scenario (solid lines). The roughness canopy region is shown in the figure as a grey shaded region. Note that the TI term has two components in rough-wall cases, the one from Reynolds (or time) averaging $\mathrm{TI_{tur}}$ and that from the intrinsic averaging or the coherent part $\mathrm{TI_{coh}}$. Notice that $\mathrm{TI_{tur}}$ acts a momentum sink and source in the outer and inner region (including the roughness canopy) respectively, whereas $\mathrm{TI_{coh}}$ also acts as a momentum sink and source, but now within the upper and lower part of the roughness canopy, and approaching zero outside the roughness canopy. Overall, the outer-region of the flow is a balance between the $\mathrm{TI_{tur}}$ and the pressure gradient, which is similar to the smooth-wall case. In the inner region, however, in the rough-wall case we have the drag owing to the roughness canopy (D_x), which dominates the rest of the terms. So, in the inner-region, canopy drag is the main momentum sink, whereas all the other terms predominantly act as a source of momentum. Note that VF in the smooth-wall case is always a momentum sink (i.e., takes only negative values), whereas here in the rough wall case we observe the interesting feature of VF acting as a momentum source within the canopy. This is because of the increasing wall-normal gradient of the mean velocity with the wall distance inside the canopy, which is contributed by the canopy recirculation region leading to a negative mean velocity deep within the canopy. Note that, in figure 2(b), $\phi_f\langle\overline{D_x}\rangle^+$ is obtained as a difference from (3), but in Appendix A, we evaluate $\langle\overline{D_x}\rangle$ directly from the DNS data as a sum of the pressure and viscous forces on the canopy walls, and it is close to that obtained from (3). Interestingly though, direct calculations where we decompose $\langle\overline{D_x}\rangle$ into pressure and viscous contributions (c.f., figure 5) shows that both contribute approximately same magnitudes towards $\langle\overline{D_x}\rangle$ with the pressure forces contributing within the canopy and the viscous forces dominating in the outer portion of the canopy.

Addition of particles in the rough-walled pipe do not substantially change the force balance within the canopy (dashed lines in figure 2b), even though both canopy drag and $\mathrm{TI_{tur}}$ seem to be slightly attenuated in magnitude by the particles. The main effect of particles are, however, in the outer region; we observe a substantial reduction in $\mathrm{TI_{tur}}$ magnitude which is compensated by the momentum sink owing to the particles. This effect is similar to the smooth-wall case, but in the rough-wall case the particles exert a much more substantial drag force on the fluid. Importantly, in contrast to the smooth-wall case, in the rough-wall case, $\int_0^R -\langle\phi_f\overline{F_{px}}\rangle r\,\mathrm{d}r < 0$ (again confirmed by the DNS) because fast-moving particles from the outer region collide with the roughness canopy, transferring momentum to the wall. This momentum gain by the particles, and hence a loss of momentum for the fluid, is manifested in the outer region.

Overall, in both the smooth and rough cases, turbulent stresses are reduced by particles, and the balance in the outer region is primarily such that particle drag and turbulent inertia counter the pressure gradient. The extent of power consumed cannot be estimated directly from the MMB, but rather by utilising the resulting mean energy equation.

4 Net power consumption and its decomposition

The net power consumption, per unit fluid volume, in a (rough) pipe flow is

$$\frac{1}{V_{\mathrm{fluid}}}\iiint_{V_{\mathrm{fluid}}}\frac{\mathrm{d}P}{\mathrm{d}x}\overline{u_x}\,\mathrm{d}V = \frac{\mathrm{d}P}{\mathrm{d}x}\frac{\int_0^R\langle\overline{u_x}\rangle\phi_f\,r\,\mathrm{d}r}{\int_0^R\phi_f\,r\,\mathrm{d}r} = \frac{\mathrm{d}P}{\mathrm{d}x}U_b, \quad (5)$$

where, V_{fluid} is the total fluid region within the pipe, and the bulk velocity $U_b \equiv \frac{\int_0^R\langle\overline{u_x}\rangle\phi_f\,r\,\mathrm{d}r}{\int_0^R\phi_f\,r\,\mathrm{d}r} = \frac{\int_0^R\langle\overline{u_x}\rangle\phi_f\,r\,\mathrm{d}r}{R_{\mathrm{eq}}^2/2}$, using the definition of R_{eq} and noting that the fluid volume $V_{\mathrm{fluid}} = L_x 2\pi\int_0^R\phi_f\,r\,\mathrm{d}r = L_x\pi R_{\mathrm{eq}}^2$.

Starting from (3), and using (5), an appropriate mean energy equation can be derived that decomposes the net power consumed into contributions from mean dissipation, turbulent (Reynolds and coherent) dissipation, and work done in overcoming canopy drag and in moving particles. The radial distributions of these are presented in figures 3(a) and (b) and their integral contributions in figure 4. Again in figures 3(a) and (b) the solid and dashed lines are respectively unladen and particle-laden cases.

In figure 3(a) for smooth pipes, although the particles transfer no net momentum to the wall, the integral which represents the power consumption by the particles is non-zero (i.e., integral of the black dashed lines in figure 3a is positive), consistent with fact that particles require energy expenditure to be carried through the fluid. In fact, as figure 4 (second bar)

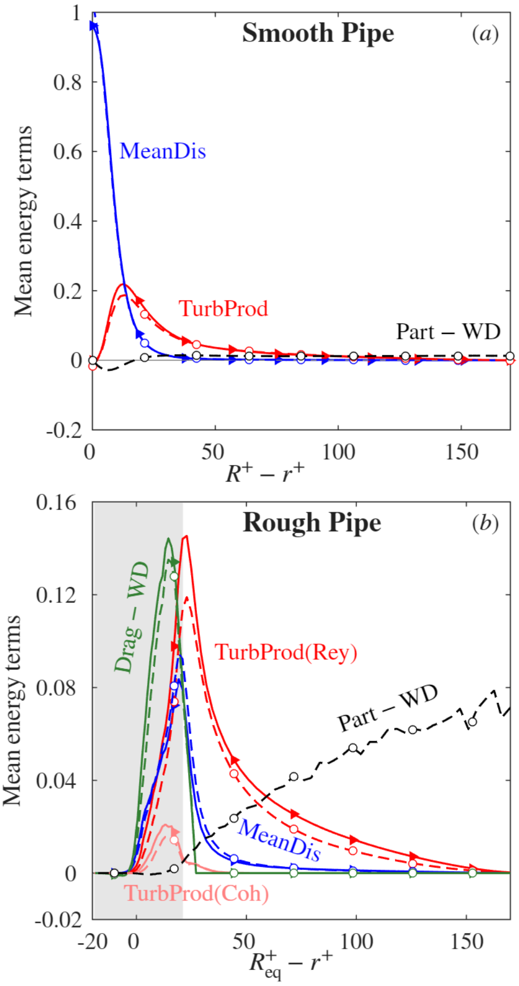

Figure 3. Profiles of the terms in mean rate of energy equation respectively for smooth and rough pipes. Solid lines are unladen, whereas dashed lines correspond to particle-laden cases. The different contributions are from the mean dissipation: MeanDis, turbulent production from Reynolds stresses – TurbPro(Rey), turbulent production from coherent stresses: TurbPro(Coh), work done by the canopy drag: Drag-WD, and work done in moving the particles: Part-WD. The shaded region in (b) corresponds to the roughness canopy.

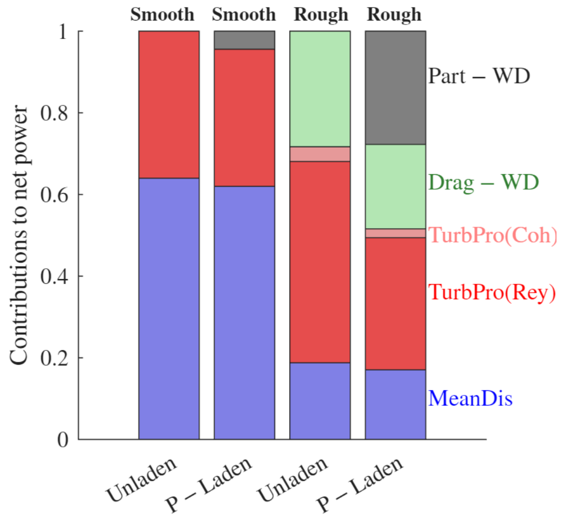

Figure 4. Radial integral, i.e, $\int_0^{R^+}(\ )r^+\,\mathrm{d}r^+$, of the distributions in figure 3(a) and (b) normalised by the total power consumption per unit volume (in viscous scaling) $U_b^+ R_{\mathrm{eq}}^+$, where U_b is the bulk velocity.

shows, particles consume about 5% of the total energy, which comes at the expense of reducing the energy loss by the turbulence.

In the rough pipe (c.f., figure 3b), canopy drag is a major contributor to energy loss (about 30%). Particles in a rough pipe require much more energy (compared to smooth wall) to be driven, which turns out to be about 30% of the overall pumping power (per unit volume). This is due to the particles lowering the turbulence, and hence the turbulent dissipation within the fluid (c.f., figure 4, the last vertical bar). Overall, in going from smooth to rough, the major change is the reduction in energy loss by the mean viscous gradients that is replaced by energy lost in the canopy drag of the rough pipe. The shift from unladen to particle-laden flow results in only a small reduction in the turbulence (see figure 3b), but a noticeable reduction in the energy lost to the turbulence, with hardly any effect on the mean or drag related dissipation. Particles, however, contribute substantially to the overall driving power. For the smooth-wall case the particles contribute relatively smaller fraction of the overall energy lost, but in rough-wall pipe the energy lost in driving the particles is relatively large. As observed in figure 4, in both smooth and rough-wall flows the energy lost to the particles is offset by the reduced losses to the turbulence.

5 Conclusion

Here we present the mean momentum (force) balance and rate of energy balance for a smooth and rough walled pipe for both unladen and for particle-laden scenarios. In both smooth- and rough-wall cases the $St^+ = 500$ and the particle volume fraction $\phi_{pv} \approx 2\times10^{-5}$. In the particle-laden smooth-wall case, although the net momentum transferred by the particles to the wall is zero (i.e., $\int_0^R \overline{F_{px}}\, r\,\mathrm{d}r = 0$) as shown in figure 2(a), particles extract a non-zero net power (c.f., figure 3a) of about 5% (c.f., figure 4) from the fluids. In rough-walled particle-laden flows, particles extract both momentum and energy from the fluid. Axial particle momentum is lost because of the collision of particles with the roughness canopy, even though the manifestation of this momentum loss within the fluid happens in the outer region of the flow outside the roughness canopy. The energy required to transport the particles in a rough-walled pipe is substantial, and for our case it is about 30% (compared to about 5% in smooth-walled pipes).

Appendix A

The purpose of this appendix is to present the procedure undertaken using the DNS data to calculate the pressure and viscous forces within the small radial strip of volume V_f (c.f., equation 4b). We will then compare, (i) the radially dependent drag force that we can obtain as a difference from the pipe MMB equation (3) for the unladen case with that obtained directly from DNS using (4b), and (ii) the direct calculation of the total volume-integrated forces with the pressure drop driving the flow.

Using DNS data (i.e., local surface pressure and velocity

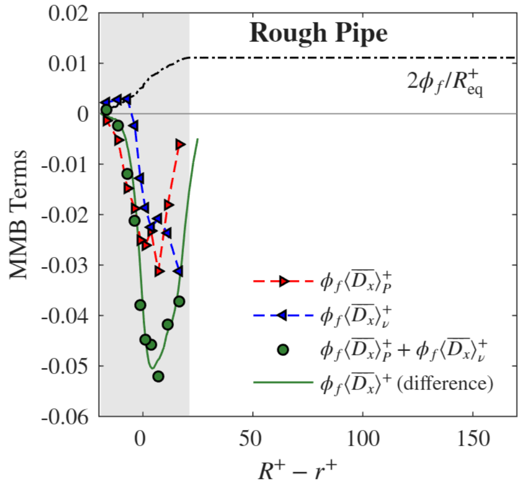

Figure 5. Drag terms in the MMB equation for the unladen rough-wall case. The symbols show drag evaluate using the DNS data surface integration as in (7), whereas the solid line is drag evaluated as a *difference*, i.e, using the RHS terms of (8) which is the same as (3) for an unladen case.

gradient) we calculate the forces on the RHS of (4b),

$$\underbrace{\iint_A (-\overline{p}n_x)\, dA}_{F_P} + \underbrace{\iint_A (\mu\nabla\overline{u_x}\cdot n)\, dA}_{F_\nu} = V_f\langle\overline{D_x}\rangle, \qquad (6)$$

where, recall, that A is the area surrounding V_f where the fluid is in contact with the solid, and F_P and F_ν are respectively the pressure and viscous forces from the DNS. The drag force appears in the pipe MMB (3) as $\phi_f\langle\overline{D_x}\rangle$, where $\phi_f = V_f/V_0$ with $V_0 = 2\pi r\Delta r L_x$ and Δr representing the thickness of the radial strip. Hence,

$$\begin{aligned}
\phi_f\langle\overline{D_x}\rangle &= \frac{V_f}{V_0}\left(\frac{1}{V_f}(F_P+F_\nu)\right)\\
&= \frac{1}{V_0}(F_P+F_\nu)\\
&= \frac{F_P}{2\pi r\Delta r L_x} + \frac{F_\nu}{2\pi r\Delta r L_x}, \text{ or,}\\
\phi_f\langle\overline{D_x}\rangle^+ &= \underbrace{\frac{F_P/\left(\rho u_\tau^3/\nu\right)}{2\pi r\Delta r L_x}}_{\phi_f\langle\overline{D_x}\rangle^+_P} + \underbrace{\frac{F_\nu/\left(\rho u_\tau^3/\nu\right)}{2\pi r\Delta r L_x}}_{\phi_f\langle\overline{D_x}\rangle^+_\nu}
\end{aligned} \qquad (7)$$

Now, the MMB drag contribution $\phi_f\langle\overline{D_x}\rangle^+$ can be also be calculated as a 'difference' using (3), which for an unladen case is,

$$\phi_f\langle\overline{D_x}\rangle^+ = \phi_f\frac{2}{R^+_{eq}} + \frac{1}{r^+}\frac{d}{dr^+}\left(r^+\phi_f\left[\langle\overline{\tau_{xr}}\rangle^+ + \frac{d\phi_f\langle\overline{u_x}\rangle^+}{dr^+}\right]\right), \qquad (8)$$

where the RHS of the (8) is evaluated using the data.

Figure 5 shows the comparison of $\phi_f\langle\overline{D_x}\rangle^+$ calculated as a difference using (8) in a solid line with direct surface integration (7) in symbols. The solid line is in good agreement with the circular symbols representing the sum of the pressure and viscous components. We note that deep within the roughness canopy the mean velocity changes sign, i.e., the flow is backwards representing a recirculation region, which gives rise to a *positive* viscous drag (c.f., the $\phi_f\langle\overline{D_x}\rangle^+_\nu$ in figure 5). At most locations within the canopy the pressure drag ($\phi_f\langle\overline{D_x}\rangle^+_P$) dominates the viscous drag ($\phi_f\langle\overline{D_x}\rangle^+_\nu$) except towards the outer edge of the canopy where the smoother and relatively flat nature of our 'egg-carton' roughness results in an increased viscous drag compared to the pressure drag.

In an unladen flow, a global measure of the accuracy of the pressure and surface drag is that the sum should equal to the net pressure-gradient driving force applied to the fluid. Integrating (8) over the pipe, i.e., $\int_0^{R^+}(8)\, r\, dr^+$ leads to :

$$\begin{aligned}
\frac{2}{R^+_{eq}}\int_0^{R^+}\phi_f r^+ dr^+ &= \int_0^{R^+} r^+\phi_f\langle\overline{D_x}\rangle^+ dr^+\\
\frac{2}{R^+_{eq}}\frac{R^{+2}_{eq}}{2} &= \int_0^{R^+}(u_\tau/\nu)^2 r\left(\frac{(F_P+F_\nu)/\left(\rho u_\tau^3/\nu\right)}{2\pi r\Delta r L_x}\right) dr\\
R_{eq}\frac{u_\tau}{\nu} &= \frac{1}{\rho u_\tau \nu}\sum\left(\frac{(F_P+F_\nu)}{2\pi L_x}\right)\\
R_{eq}\rho u_\tau^2(2\pi L_x) &= \sum(F_P+F_\nu)
\end{aligned} \qquad (9)$$

where we have used the definition of R^+_{eq}, i.e., $\int_0^{R^+}\phi_f r^+ dr^+ = R^{+2}_{eq}/2$. The LHS of (9) for our case (where $u_\tau = \rho = 1$, $R_{eq} = 0.5$) is πL_x, and numerical evaluation of the RHS term using DNS shows that the RHS differs from the LHS by about 0.15%, which is small. From a practical point of view, calculation of the integrals F_P and F_ν requires a small radial distance (Δr^+), and by trial and error, we have found that $\Delta r^+ \approx 2$ provides reasonably smooth radial profiles of the F_P and F_ν, whereas a much smaller Δr^+ results in profiles that oscillate, but they still satisfy (9).

REFERENCES

Chan, L, Zahtila, T, Ooi, A & Philip, J 2021 Transport of particles in a turbulent rough-wall pipe flow. *J. Fluid Mech.* **908**, A1.

Chin, C, Philip, J, Klewicki, J, Ooi, A & Marusic, I 2014 Reynolds-number-dependent turbulent inertia and onset of log region in pipe flows. *J. Fluid Mech.* **757**, 747–769.

Cui, G, Emadzadeh, A, Ooi, A & Philip, J 2025 Experimental study of inertial particles in a horizontal turbulent pipe flow: neutrally buoyant and denser-than-fluid particles. *J. Fluid Mech.* **1008**, A2.

Cui, G, Emadzadeh, A, Xu, Z, Monty, J & Philip, J 2026 Experimental study of particle-laden turbulent horizontal pipe flows up to $Re_\tau \approx 2000$ in the two-way coupling regime. *Int. J. Multiph. Flow* **197**, 105591.

Gualtieri, P., Battista, F., Salvadore, F. & Casciola, C.M. 2023 Effect of stokes number and particle-to-fluid density ratio on turbulence modification in channel flows. *J. Fluid Mech.* **974**, A26.

Morrill-Winter, C, Philip, J & Klewicki, J 2017 An invariant representation of mean inertia: theoretical basis for a log law in turbulent boundary layers. *J. Fluid Mech.* **813**, 594–617.

Nikora, V *et al.* 2007 Double-averaging concept for rough-bed open-channel and overland flows: Applications. *J. Hydraul. Eng.* **133** (8), 884–895.

Picano, F., Breugem, W. P. & Brandt, L. 2015 Turbulent channel flow of dense suspensions of neutrally buoyant spheres. *J. Fluid Mech.* **764**, 463–487.

Unigarro Villota, S, Ghisalberti, M, Philip, J & Branson, P 2023 Characterizing the three-dimensional flow in partially vegetated channels. *Water Resour. Res.* **59** (1), e2022WR032570.

Wei, T, Fife, P, Klewicki, J & McMurtry, P 2005 Properties of the mean momentum balance in turbulent boundary layer, pipe and channel flows. *J. Fluid Mech.* **522**, 303–327.

Zahtila, T, Chan, L, Ooi, A & Philip, J. 2026 Turbulent pipe and channel flows modulated by heavy inertial particles: comparison of geometries and decomposition of net drag and power consumption. *under preparation* .